

On the Role of Ambient Environments in the Collapse of Bonnor-Ebert Spheres

Erica Kaminski¹, Adam Frank¹, Jonathan Carroll¹, Phil Myers²

ABSTRACT

We consider the interaction between a marginally stable Bonnor-Ebert (BE) sphere and the surrounding ambient medium. In particular, we explore if and how the in-fall from an evolving ambient medium can trigger the collapse of the sphere using 3-D AMR simulations. We study BE sphere dynamics when ambient densities range from the previously explored 'sparse' values ($\rho_{amb} = 0.01\rho(R_{BE})$ where R_{BE} is the BE sphere's truncation radius), to values equal to that at the sphere's outer most edge ($\rho_{amb} = \rho(R_{BE})$). We find the resulting collapse dynamics to vary considerably with ambient density. In the highest ambient density cases, in-falling material drives a strong compression wave into the cloud. It is the propagation of this wave through the cloud interior which triggers the subsequent collapse. In contrast, for the lower ambient densities, we find the main trigger of collapse to be a quasistatic adjustment to the gravitational settling of the ambient gas, which eventually renders the BE sphere super-critical. In addition, we find that all cases assume the classic 'outside-in' behavior before a protostar (i.e. sink particle) forms, even in the strong compression wave dominated cases. Our work supports scenarios in which BE dynamics begin with an early compression-wave/in-fall phase and only later assumes the "classic" super-critical collapse mode.

Subject headings:

1. Introduction

"Bonnor-Ebert"(BE) spheres (Bonnor 1956; Ebert 1955) have long been a favorite candidate for initial conditions in studies of star formation (Hunter 1977; Foster 1994; Banerjee et al. 2004). These non-singular, isothermal, hydrostatic solutions to the self-gravitating fluid equations are constructed to be in pressure equilibrium with an ambient environment making them an effective "toy-model" for investigations of protostellar collapse. In addition, even though BE spheres represent highly simplified solutions to these equations, observations have shown some quasi-spherical clumps to match the hydrostatic equilibrium (HSE) of BE solutions (*i.e.* the Bok Globule B68 (Alves et al. 2001)).

In terms of theoretical studies, a particularly useful property of BE spheres are their well-established stability criterion. Isothermal, hydrostatic spheres with density contrasts below 14.5 are stable against gravitational contraction (first shown by Bonnor (1956); Ebert (1955)). This simple stability condition can be cast in terms of a critical mass (M_{BE}), similar to the Jeans mass (M_J) but with a slightly different numerical coefficient (e.g. for the critical BE sphere, $M_{BE} \sim 2 M_J$ of a uniform, isothermal sphere of equal temperature and external pressure). Such a critical mass provides an easy interpretation of the relative

¹Department of Physics and Astronomy, University of Rochester, Rochester, NY 14620
Email contact: erica@pas.rochester.edu

²Harvard-Smithsonian Center for Astrophysics, 60 Garden Street, Cambridge, MA 02138, USA
Email contact: pmyers@cfa.harvard.edu

importance of thermal and gravitational energies within the sphere, or assumed "pre-protostellar core" (a phrase coined by Ward-Thompson et al. (2007)). Once this stability condition is violated, collapse is triggered.

While the initial properties of isothermal spheres are easily derived analytically, deriving analytical models for their collapse has not been trivial. Because of this, it has been part of an on-going debate about the true nature of the mechanisms involved in isolated star formation. Modern studies of the detailed dynamics of protostellar cloud collapse date back to work by Larson and Penston (LP) who explored similarity solutions for uniform initial density clouds ((Larson 1969; Penston 1969)). Later, Shu presented the "expansion wave" similarity solution for singular ($\rho \propto r^{-2}$) isothermal spheres (SIS) (Shu 1977). The Shu solution described the collapse of the infinitely centrally condensed SIS, whose center immediately collapses into a constant-accreting point mass. This type of core formation results in an *inside-out* collapse; adjacent shells collapse one after the next in an outward propagating expansion wave of lost pressure support. Shu and collaborators (Shu et al. 1987; Shu & Adams 1987) suggested this inside-out collapse would occur for *any* hydrostatic, isothermal, spherically-symmetric distribution, including Bonnor-Ebert spheres. This was speculated to occur through a subsonic approach from the flat-topped density distribution of the BE sphere to the r^{-2} density law characteristic of the SIS. After a sufficient perturbation, it was assumed inside-out collapse would be initiated.

Simulations of isolated, unstable BE spheres, however, showed very different behavior than an outward-propagating rarefaction (Hunter 1977; Foster 1994; Banerjee et al. 2004). Unlike the SIS, the BE sphere appears to collapse from the *outside-in*. This non-homologous collapse is characterized by an inward-directed flow beginning in the outer regions of the cloud (beyond the flat-topped 'core' region of the BE sphere). The profile which develops shows a flat-topped core that increases in density while shrinking in radial extent. The density of the core, ρ_0 , increases as its radius decreases. Beyond the core an extended envelope with a r^{-2} profile develops. Once a central point mass has formed, the mass accretion rate onto the central object declines with time. This outside-in collapse is what we will call "classic" evolution of an unstable BE sphere. Simulations have shown this to be the general progression of BE collapse, irrespective of perturbation type, degree of central concentration, and outer boundary conditions (Hunter 1977; Foster & Chevalier 1993; Banerjee et al. 2004; Anathpindika & Di Francesco 2013).

The complexity of dynamics shown in simulations has made it challenging to reconcile the BE sphere collapse with the early similarity solutions. In Whitworth & Summers (1985) (from here on referred to as WS) a general set of similarity solutions for the isothermal sphere were derived, with the Shu and LP solutions appearing at varying limits. The WS solutions describe the collapse as either being triggered or enhanced by an externally driven, inward propagating compression wave, depending on the degree of initial stability of the sphere. In early eras of the flow, i.e. in regions or times before the traversal of the compression wave, the sphere is either in a static equilibrium state (that may be oscillating internally via sound waves, i.e. the marginally stable BE sphere), or condensing because it is initially far out of equilibrium (e.g. uniform sphere). The head of the compression wave represents a region of enhanced density that propagates deeper into the sphere, and its strength depends on the degree of external pressure at the sphere's surface. Once the compression wave converges on the center, a central accreting object forms.

A number of authors have since studied the BE collapse problem in the WS compression wave framework. For instance, Hennebelle et al. (2003) looked at the effect of differentially increasing the external pressure on marginally stable BE spheres. The rate at which they increased the external pressure varied in their runs, which allowed them to infer a general trend: an inward propagating compression wave was induced at the BE surface that later converged on the center and resulted in a centrally accreting point mass. The

strength of the compression wave varied depending on the magnitude and duration of the pressure increase, in line with the WS model. Anathpindika & Di Francesco (2013) also studied the collapse of the BE sphere in terms of a compression-wave scenario. By placing a BE sphere in a warm, sparse ambient medium in pressure equilibrium with the sphere, they triggered collapse by reducing the thermal energy inside the sphere’s interior, triggering compression wave dynamics that in some cases amplified condensation and led to collapse, while in other cases only triggered oscillations.

It is noteworthy that despite the great deal of attention paid to BE spheres, both analytically and numerically, studies of their basic collapse properties have placed them in a discontinuous, low-density ambient media and then perturbed them into collapse. This implies an isolation of the collapse from the ambient environment. From this, it is hard to disentangle the effect of the ambient medium, which has been included in the WS framework. Further, the effect of density mismatch between the sphere’s outer edge and its encompassing medium is also poorly understood. For instance, Myers (2008) took care in modeling the transition in density from sphere to ambient gas. In that study, where the in-fall and dispersal of ambient gas onto BE spheres was calculated, Myers underscored the importance in considering this density transition. It thus seems an interesting and previously unexplored topic to *not* isolate the BE sphere in studying its collapse, and instead consider the role the *ambient* medium plays in that collapse. From a purely theoretical perspective, one can ask under what conditions does the ambient evolution alone lead to BE sphere collapse, and how does this collapse change with different density contrasts between sphere and ambient. To this end, we studied the special case of placing a BE sphere in the center of mass position of concentric, homogenous molecular clouds of various densities and watching the system’s natural evolution with no added perturbations.

Maybe save this detail for the discussion– discontinuous transitions in density may be physically plausible when clouds form via dynamical interaction (i.e. isolated clumps near irradiating pressure sources).

2. Methods

2.1. Bonnor-Ebert sphere definitions

Here we briefly restate definitions for the critical BE sphere. The well known derivations (REF Chandrasekhar and others here?) are included in the Appendix 7.3 for completeness. All BE spheres show a flat-topped density profile near their centers with outer densities that decline monotonically with radius (Fig. 1). The BE sphere, defined by its truncation radius (R_{BE}) and confining pressure ($P(R_{BE})$), is thermally or gravitationally dominated depending on the value of its non-dimensional radius,

$$\xi = \left(\frac{4\pi G\rho_0}{C_s^2}\right)^{1/2}r \quad (1)$$

The sphere is semi-stable, i.e. on the cusp of its stability curve, when its $\xi = 6.5$. At this point, with no added perturbation, the sphere may oscillate gently about its equilibrium. Likewise, collapse can ensue in this state with the application of small perturbations. The critical values of external pressure and radius of such a marginally stable BE sphere of mass M_{BE} and with isothermal sound speed C_s are (Spitzer 1968):

$$r_{crit} = 0.41 \frac{GM_{BE}}{C_s^2} \quad (2)$$

$$P_{crit} = 1.40 \frac{C_s^8}{G^3 M_{BE}^2} \quad (3)$$

To initialize our simulations we used an approximate analytical solution of the Lane-Emden equation (Liu 1996), which requires inputs of dimensional radius (R_{BE}), non-dimensional radius (ξ) and central density (ρ_0)². The output is the density profile $\rho(r)$, which given the assumption of isothermality, yields the pressure profile $P(r)$ as well.

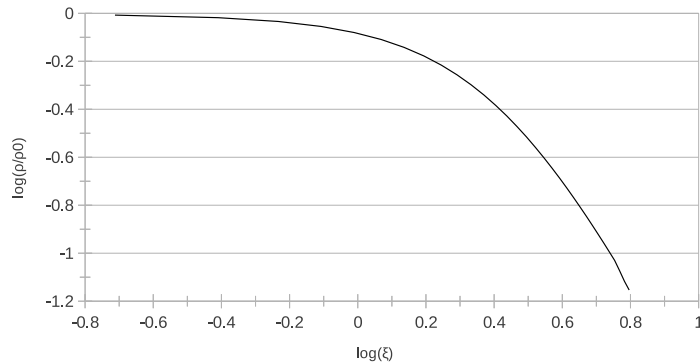


Fig. 1.— The density profile of a critical Bonnor-Ebert sphere as a function of ξ in log-log space. The y-axis is in scaled units, normalized to the central density ρ_0 of the BE sphere. Given the scaled nature of this curve, it represents a family of solutions, each BE sphere given by a different ρ_0 and truncation radius.

2.2. Model

We modeled the collapse of the marginally stable BE sphere ($\xi = 6.5$) using AstroBEAR2.0³, a highly parallelized, multidimensional, adaptive mesh refinement (AMR) code that solves the equations of hydrodynamics and magnetohydrodynamics on a cartesian grid (Cunningham et al. 2009; Carroll-Nellenback et al. 2011). AstroBEAR2.0 has a library of multiphysics tools, including heat conduction, resistivity, radiative cooling and self-gravity. In the present work, AstroBEAR2.0 solved the Euler equations with self-gravity. The Poisson solver for self-gravity uses HYPRE⁴, a software package that solves linear systems on massively parallelized systems. Our methods for self-gravity are described in Appendices (7.1-7.2).

The problem domain was a cube of side length L , with the BE sphere at the center. We chose to initialize the fluid variables with the same values given in Banerjee et al. (2004), hereafter ‘BPH04’, to verify the output of our code. Those authors chose parameters to match potential sites of massive star formation. Thus, our BE sphere has an initial radius of $R_{BE} \approx 1.62 pc$, central density $n_0 = 2004$, temperature $T = 20$ K, mass $M_{BE} = 151 M_\odot$, and isothermal sound speed $C_s \sim 0.4$ km/s. It is initialized to be in pressure equilibrium with the ambient. The gas in the box was assumed to be atomic hydrogen ($\mu = 1$), with a ratio

²documentation: <https://clover.pas.rochester.edu/trac/astrobear/wiki/u/BonnorEbertModule>

⁴documentation: <https://computation.llnl.gov/casc/hypre/software.html>

of specific heats of ($\gamma = 1.0001$) to approximate an isothermal equation of state. Given pressure equilibrium, the ambient medium and BE sphere will begin with different temperatures if there is a density mismatch at their boundary. However, the simulation evolves effectively isothermally. Note that the AMR allows us to place the boundaries of the domain far from the edge of the BE sphere with $L = 30 R_{BE}$.

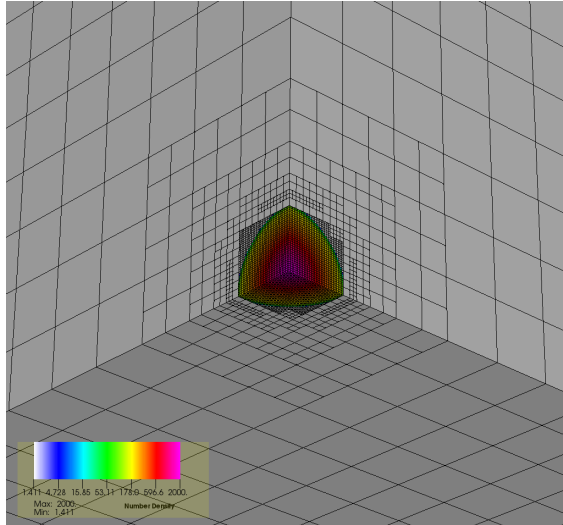


Fig. 2.— Schematic of the mesh with an octant of the Bonnor-Ebert sphere located at $(0,0,0)$. While all simulations were initialized with 5 levels of refinement to achieve ~ 34 cells per initial clump radius, only the first 3 levels are plotted here for clarity. The mesh was dynamic in that additional levels of refinement were added as needed (see text). The color-bar shows variation in n (cm^{-3}). Note that the maximum value in this plot is lower than the reported $2004 cm^{-3}$, given the data from the finest cells are not plotted.

For this study we placed the BE sphere at the origin of a spherically symmetric mass distribution inside of the simulation box. This is a special case, and models an embedded core (the BE sphere) that is located at the center of mass position of an encompassing, concentric molecular cloud complex. If the parent cloud is gravitationally unstable, its collapse path will be toward the center of the box, coinciding with that of the collapsing BE sphere. For density mismatch at the boundary, this implies a process to have dispersed gas isotropically around the BE sphere, such that the encompassing cloud is of a uniformly lower density. This is an idealization that may mimic uniformly distributed H₂ regions around the embedded core. We varied the degree of density discontinuity at this edge to observe the strength of interaction between parent cloud and embedded core. (Should we add anything more here - such as how you might imagine the matched case as forming, or anything on doing a more general case?)

Given the symmetry of the problem we only simulated the 1st (positive) octant of the domain with the simulated domain extending from $[0,25pc]$ in x -, y -, and z - directions and the BE sphere centered at $(0,0,0)$ (currently AstroBEAR is not configured in spherical coords: Figure 2). Boundary conditions on the box were set to extrapolating (outflow) on all outside-facing sides, and reflecting on the faces that sliced through the BE sphere. The coarse grid was made up of 16^3 cells, initialized with 5 levels of AMR within the BE sphere. Each level of AMR increased the effective number of cells in each direction by a factor of 2. Thus, at the start of the simulation the effective resolution was $\Delta x_{min} \approx 0.05$ pc, corresponding to ≈ 34 cells/ R_{BE} . Two additional levels of refinement were triggered during the BE sphere collapse when the "Truelove condition" (Truelove et al. 1997),

$$\Delta x > \lambda_J/4 \tag{4}$$

was violated, where λ_J is the local Jeans length associated with each cell center, and Δx is the width of a cell on any given level. Essentially this is an AMR criterion that maintains adequate resolution of the Jeans length. Once the maximum refinement is reached, sink particles are generated based on conditions described in Federrath et al. (2010). The simulations were halted after the formation of a sink.

2.3. Simulations

We performed a set of 6 simulations, listed in Table 1. In each run the marginally stable ($\xi = 6.5$) BE sphere was initialized to be in pressure equilibrium with an ambient medium of a different uniform density. To test the stability of the BE sphere, we chose an ambient density of $\rho_{amb} (r > R_{BE}) = 0.01\rho (R_{BE})$, where R_{BE} is the truncation radius of the BE sphere. This we named the "Sparse" ambient case. No perturbation was applied to the sphere and we ran the simulation out for 5 crossing times t_{sc} of the sphere,

$$t_{sc} = R_{BE}/C_s \approx 3.8 \text{ Myr} \tag{5}$$

Next we added a 10% overall density enhancement to the BE sphere and ambient in the sparse ambient case. This was the same form of perturbation BPH04 and others have used to initiate outside-in collapse. We designate this the "Classic" case. We then carried out a series of runs that placed the sphere in ambient environments of varying density. Note that no perturbations were applied in any of these runs; it was only the effect of the ambient medium on the BE sphere which drove the subsequent dynamics. The ambient density in this series ran from $\rho_{amb} = \rho (R_{BE})$ ("Matched" case) to $\rho_{amb} = 1/30 \rho (R_{BE})$ (see Table 1).

Run	Density of Ambient	Perturbation?
Sparse	$0.01\rho (R_{BE}) \approx 1.5 \text{ cm}^{-3}$	No
Classic	$0.01\rho (R_{BE})$	YES
Matched	$\rho (R_{BE})$	No
1/3	$1/3 \rho (R_{BE})$	No
1/10	$1/10 \rho (R_{BE})$	No
1/30	$1/30 \rho (R_{BE})$	No

Table 1: Description of the 6 simulations of varying background densities. The first column lists the name of the run. The second column gives the ambient density of the simulation, and the third column states whether a perturbation was applied to initiate collapse.

3. Results

3.1. A Test of Stability - Sparse Ambient Medium

As discussed in the last section, in this run the BE sphere was placed in a hot (2000 K), low density (1.4 cm^{-3}) ambient medium. The simulation was run for five sound crossing times of the sphere ($\approx 19 \text{ Myr}$, Eq. 5). Figure 3 shows the density and radial velocity profiles (averaged over angle) within $r=1.5R_{BE}$ during the simulation. Fluid motions remained subsonic and represented sound waves traveling from edge to center as

the BE sphere adjusted to the initial set-up. The sphere oscillated around its initialized equilibrium values with no indication of either collapse or unstable expansion being triggered. The largest radial excursion in the sphere’s radius represented only 10% of the initial value of R_{BE} . These results confirm the code’s ability to recover appropriate, analytical solutions for self-gravitating fluids.

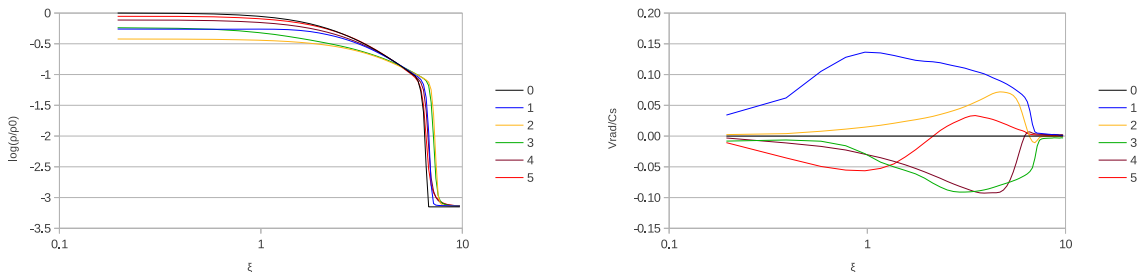


Fig. 3.— Density and radial velocity profiles for the Sparse case, $\rho_{amb} = \rho(R_{BE})/100$. The x-axis is in units of non-dimensional radius as defined by Eq. 1. The sphere’s initial outer boundary is at $\xi = 6.5$ on the x-axis and can be traced by the sharp discontinuous jump in density that occurs at the BE sphere-ambient boundary. Density and radial velocity are averaged over angle in these and all subsequent plots. As can be seen on the left, the sphere oscillated to lower $\rho(r)$, but returned close to the equilibrium profile by $t/t_{sc} = 5$. The right-hand plot shows small subsonic radial motions throughout the sphere during this time period. As usual, negative velocities indicate inward motions.

3.2. Classic Collapse

As a second test of our code, we reproduced the results of other studies of BE sphere collapse (namely, BPH04). Holding other conditions equal to the sparse case, we added a 10% density increase to the entire simulation box. This increased the mass within the sphere above that which can be supported by thermal pressure alone, as dictated by the Lane-Emden equation ($E_{th} < E_g$).

The collapse began in the outer regions of the sphere and propagated inward with time modifying the density and radial velocity profiles (Fig. 4). Note that while the times plotted in Figure 4 are given in units of t_{sc} , they are chosen relative to the formation of a sink particle. That is, the last time state plotted in Figure 4, as well as all remaining density and radial velocity plots, is equal to the moment at which a sink formed for that particular run. Figure 4 shows the characteristic changes in density for BE collapse, i.e. the monotonic increase in the density of the central flat core region. We also saw the flat core decrease in radial extent over the simulation. Outside of the core, an in-falling envelope with r^{-2} profile was formed. By $t/t_{sc} = 0.82$ a sink particle was created and the inward radial velocity had become marginally supersonic ($v_{rad} \sim 2.2C_s$), in agreement with other studies of BE collapse (Banerjee et al. 2004; Foster & Chevalier 1993; Hunter 1977). We note that the maximum density at sink particle formation depends solely on our choice of maximum refinement reached ($\Delta x \propto \lambda_J \propto \rho^{-1/2}$). Since each simulation had the same maximum level of refinement, the density that triggered the final refinement level (hence sink particle formation and end of simulation) was the same throughout the different runs, i.e. $n = 1.9 \times 10^6 \text{ cm}^{-3}$. Note this is lower than the density $n = 10^7 \text{ cm}^{-3}$ at which the isothermal assumption is no longer valid (**EK: need to cite??**).

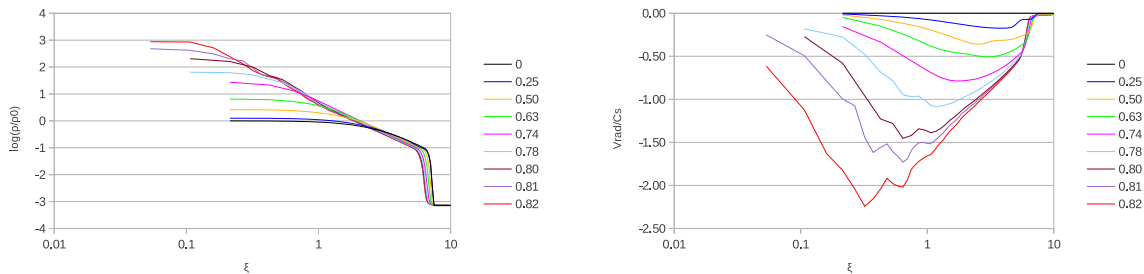


Fig. 4.— Density and radial velocity profiles for the ”Classic” case (refer to Table 1). As indicated by the left-hand density plot, outside-in collapse was established with the formation of a r^{-2} envelope trailing a flat inner collapsing core. The right-hand radial velocity profile also matches canonical outside-in collapse, marked by an inward radial flow that began at larger radii and moved inward with time. The peak velocity became marginally supersonic, approaching $\sim 2.2 C_s$ as expected (see text). The center sink particle formed by the last time state plotted in all of the figures. Here, $t_{sink}/t_{sc}=0.82$.

3.3. Collapse Under Realistic Ambient Conditions

Having established the code’s ability to recover both hydrostatic solutions and previously explored BE collapse dynamics when triggered by an arbitrary density perturbation, we explored collapse under more self-consistent conditions. To to this end we adjusted the set up of § 3.2 in two ways. First we matched the density profile across the BE sphere-ambient boundary (while maintaining pressure equilibrium at this edge), in contrast to the steep decrease in density of order 1/100 of the Classic BE model. Second, we allowed the simulation to progress without added perturbations. In addition to this ”Matched” set-up, we studied unperturbed evolution under 3 intermediate ambient densities as well, log-spaced between the Sparse and Matched density profiles.

3.3.1. Matched Ambient Medium

When the density in the ambient medium is equal to that at the outer radius of the BE sphere we see a qualitatively different behavior leading to collapse. As can be seen in the density plot (Fig. 5, left), the Matched solution is marked by an initial in-fall of material from the ambient medium onto the BE sphere. This is to be expected for two reasons. First the sphere represents a gravitating source for the ambient material. In addition, and more importantly, the higher density ambient material leads to a shorter collapse time based on its own self gravity. Given this run has the greatest ambient density, the free-fall time of the ambient is shortest, as approximated by the free-fall time of a sphere of equal radial extent and uniform density,

$$t_{ff} = \frac{1}{4} \left(\frac{3\pi}{2G\rho} \right)^{1/2} \quad (6)$$

(see Table 2). Since this timescale is on the order of the simulation time t_{sim} , and is much less than the corresponding ambient sound crossing time, it is clear that the ambient medium experiences its own homologous collapse. This is seen as the continual increase in density of material on the sphere’s outer

surface.

Run	t_{ff}	t_{sim}	t_{sc}	Dominate energy in ambient?
Classic	41.5 Myr	3.3 Myr	6.1 Myr	Thermal
Matched	4.4 Myr	3.7 Myr	57.5 Myr	Gravitational
1/3	7.8 Myr	4.9 Myr	33.1 Myr	Gravitational
1/10	13.8 Myr	7 Myr	19.2 Myr	Grav and Therm Comparable
1/30	24.4 Myr	12.2 Myr	10.5 Myr	Thermal

Table 2: Thermal and gravitational timescales for the ambient are compared to each other and the simulation time for the different runs. The free-fall time (t_{ff}) is calculated using Eqn. 6 for a uniform sphere, where the ambient density is used. Given the relative volumes of the ambient and sphere, this is to good approximation. The sound crossing time (t_{sc}) is calculated using Eqn. 5 with $r=25$ pc ($L/2$) and C_s of the ambient. When $t_{ff} \ll t_{sc}$, sound waves are unable to equilibrate the fluid and collapse ensues; the material is Jeans unstable. As can be seen from this table, t_{ff} is shortest relative to t_{sc} for the Matched case, and hence homologous collapse of the ambient is most exaggerated in this run. Collapse of the ambient becomes less apparent as ρ_{amb} decreases and t_{ff} lengthens. Sparse run not shown here for redundancy.

The evolution in the Matched case is, therefore, dominated in the early stages by the in-fall of the ambient medium. In Figure 5, we see negative velocities (in-fall) develop in the ambient gas once the simulation is initiated. Thus, material initially builds up on the surface of the BE sphere and it is both the gravitational force of this material (**EK: ?**) and its inward directed ram pressure that eventually overwhelms the sphere and drives it into collapse. The explicit agent initiating collapse in this case, however, is an inward directed compression wave induced at the BE sphere surface.

Examining the profiles for $t = 0.3 t_{sc}$, we see ambient gas has rained down on the the BE sphere, increasing the density at its outer edge. In particular, the inflection of the density representing the transition from the BE sphere to ambient gas was pushed outward from $r = 1.62pc = R_{BE}$ ($\xi = 6.5$), to $r \approx 2pc$ ($\xi \approx 8$). This represents a shell of new material that has been added to the BE sphere, which acoustic waves must initially attempt to redistribute. By $t = 0.75 t_{sc}$, the outer radius of the BE sphere (the location of the kink in density) has returned to its initial value, however, a strong peak in the density profile at $r \approx 0.6pc$ ($\xi \approx 2.5$) is now apparent, representing an inward traveling compression wave. Note that as ambient material falls inward from larger radii, the density at the boundary increases, as would be expected for the collapse of a homologous sphere. Thus, the BE sphere finds itself being crushed by an inflow of ever increasing density. We note that consideration of the ambient flow on larger scales confirms it takes the form of a homologous collapse.

By $t = 0.88 t_{sc}$, the compression wave within the sphere has altered the density of what remained of the original BE density profile. By $t = 0.94 t_{sc}$, the dynamics *switches to that of the Classic collapse*. Namely, a flat inner core region developed, surrounded by a decreasing power law envelope. The classic outside-in evolution followed; the inner flat core increased in density and shrank in radial extent while the outer regions formed an in-falling envelope whose density profile did not change. A sink particle eventually formed in the inner most cell of the simulation by $t=0.97 t_{sc}$ (14% longer than in the Classic case).

Consideration of the radial velocity profiles also demonstrates the turn-over from the the compression wave phase to the later Classic outside-in phase. During the compression wave phase ($t/t_{sc} = 0-0.88$), inward directed fluid motions originated in the ambient gas. These negative velocity regions moved inward with the peak of the compression wave. By about $0.5 t_{sc}$, the flow became supersonic. For most of the early evolution, the highest velocities are seen in the in-falling ambient gas. By $t/t_{sc}=0.94$, however, an in-falling

envelope in the BE sphere has been established. By the time of sink formation, the peak velocity inside the sphere corresponded with the edge of the flat core region, as in the Classic case. In contrast, however, this flow had a peak mach number of $M \sim 7$, compared to $M \sim 2.2$ as in the Classic simulation.

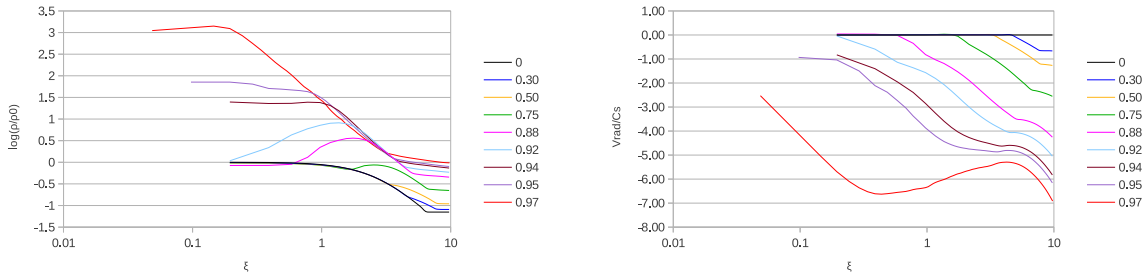


Fig. 5.— Density and radial velocity profiles for the Matched run, $\rho(R_{BE}) = \rho_{amb}$. The density profile (left) shows material building up on the BE sphere that eventually exceeded interior densities. At that time, the accumulated mass was no longer supported by thermal pressure and was driven inward via a compression wave. By $t/t_{sc}=0.94$ the density profile began to mimic the Classic collapse result. The radial velocity plot (right) shows fluid motions tied to those regions of the BE sphere where material was being redistributed. As in the density plot, late time states show velocity profiles resembling the Classic results within $\xi \approx 3$ by $t/t_{sc}=0.94$.

Thus, collapse was triggered in the Matched case by the ambient gas without an applied perturbation. To explore the limits of this ambient triggering, we next simulated the critical BE sphere embedded in ambient backgrounds of intermediate densities between the Matched and Sparse cases. These were cases '1/3', '1/10', and '1/30', corresponding to $\rho_{amb} = \rho(R_{BE})/3$, $\rho(R_{BE})/10$, and $\rho(R_{BE})/30$, respectively.

3.3.2. Intermediate Run 1/3

Evolution of the BE sphere in the densest of our Intermediate runs ($\rho_{amb} = \rho(R_{BE})/3$) proceeded similarly to the Matched case, but on different timescales. Consideration of the density plots in Figure 6 shows an initial accumulation of ambient material on the BE sphere-ambient boundary (which can be tracked by the discontinuity at this edge). By $t/t_{sc} = 0.75$ the BE sphere had both decreased in radial extent as well as increased in density at its outer edge (via a subsonic adjustment, evident in the corresponding radial velocity profile). As material continued to rain down on the BE sphere, its outer radius decreased and mass accumulated in its outer regions ($t/t_{sc} = 0.98$). The coeval velocity profiles show the flow to be subsonic up to and including this time. Thus, we see what appears to be a subsonic compression propagating inward from the (shrinking) outer radius of the BE sphere.

Without incorporating the new ambient material into an approximate HSE distribution, the sphere would become too massive to support itself against self gravity. Thus, we see collapse initiated at ($t/t_{sc} = 1.13$). As in the Matched case above, the collapse resembled the classic BE collapse in this later phase of evolution ($t/t_{sc} = 1.13-1.26$). As can be seen in the density plots, elements of the Classic collapse, such as a shrinking inner flat core trailed by a $\sim r^{-2}$ envelope, are associated with what appears to be a smaller and denser counterpart to the original BE sphere. The velocity profiles in this phase of evolution are also approaching the outside-in profiles within this "modified" BE sphere for $\xi < 4$. Recall, $\xi = r(4\pi G\rho_0)^{1/2}/C_s$,

where ρ_0 denotes the *initial* central density.

Compared to the Matched case, there are some important points to note. First, the relative times for each phase of the evolution are different. For the Matched case, the compression phase corresponds to the early equilibration and subsequent compression wave propagation. This is the dominant phase of the Matched Case evolution, taking up a larger fraction of the total simulation time. In other words, the simulation switched to the Classic phase later in time in the Matched case than in Run 1/3. This occurred because of the stronger perturbation afforded by the ambient material in the Matched case. Second, the slower flow in Run 1/3 (only marginally supersonic) led to a longer collapse time (i.e. the time until sink particle formation) of $t_{sink}/t_{sc} = 1.26$ compared to the Matched case's $t_{sink}/t_{sc} = 0.97$.

It is also interesting to note that Run 1/3 was comparable to the Classic collapse in a number of ways. If we assign the beginning of the Classic collapse phase for Run 1/3 to be $t/t_{sc}=1.19$, we see an associated $\text{Log}(\rho/\rho_0) \sim 1.2$ and $v_{rad}/C_S \sim -1.25$. Looking at the same part of the evolution in the Classic case (now corresponding to $t/t_{sc}=0.78$), we see that $\text{Log}(\rho/\rho_0) \sim 1.8$ and $v_{rad}/C_S \sim -1.1$. By the end of the simulation, the peak velocities are nearly the same, $v_{rad}/C_S \sim -2.25$, although again the simulation evolved over longer time scales for this Intermediate case compared to the Classic case, which had $t_{sink}/t_{sc} = 0.82$. Thus, once the perturbation provided by the ambient gas was established, the flow proceeded as in the Classic case.

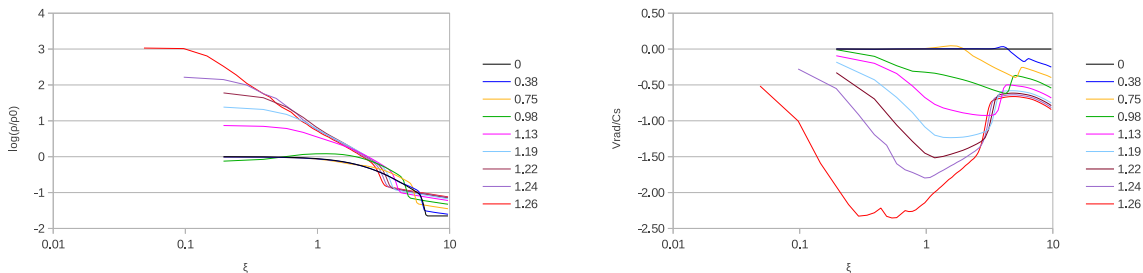


Fig. 6.— Density and radial velocity profiles for Run 1/3. A weak density wave travelled through the BE sphere after the ambient material sufficiently collected at the BE sphere surface ($t/t_{sc} = 0 - 0.98$), as can be seen in the left-hand plot. The BE sphere was squeezed into a smaller radius with increased density, driving gravitational instability that resulted in collapse. Collapse ensued in a Classic outside-in manner, as evident by the skinking flat core region and extended r^{-2} envelope ($t/t_{sc} = 1.13 - 1.26$). Coeval radial velocity profiles (right) show the flow to slowly become marginally supersonic and approach Classic results inside a truncated region of the initial BE sphere.

3.3.3. Intermediate Run 1/10

In a sparser ambient medium of $\rho_{amb} = \rho(R_{BE})/10$, the evolution and the collapse of the BE sphere proceeded qualitatively differently than in the Matched and 1/3 Runs. In the density plot of Figure 7, we see less accumulation of material on the outer surface of the BE sphere at $t/t_{sc} = 0.55$. The increase in density there contributed to a slight gravitational contraction that reduced the BE sphere radius ($t/t_{sc} = 1.10$). Further accumulation of ambient material falling onto the BE sphere after this time was negligible, yet the sphere continued to contract. As inner regions grew in density ($t/t_{sc} = 1.42$) the sphere eventually began to collapse under self-gravity when it exceeded its critical mass. The collapse then proceeded classically until

sink particle formation at $t_{sink}/t_{sc} = 1.83$.

Consideration of the velocity profiles in Figure 7 shows a subsonic adjustment of the BE sphere to material accumulating on its surface ($t/t_{sc} = 0.55$). By $t/t_{sc} = 1.42$, outside-in collapse is clearly underway, reaching a peak velocity close to the Classic result of $v_{rad}/c_s \sim -2.5$ by sink particle formation as in run 1/3.

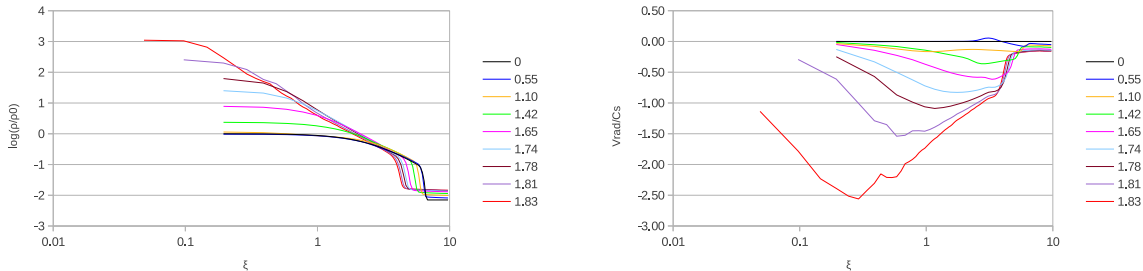


Fig. 7.— Density and radial velocity profiles for Run 1/10, $\rho_{amb} = \rho(R_{BE})/10$. A light rain of ambient material accumulated on the BE sphere surface ($t/t_{sc} = 0.55$) as can be seen in the density plot, left. The coeval radial velocity plot, right, shows small subsonic adjustments to this ambient flow. Amassed material squeezes the BE sphere into a smaller radial volume ($t/t_{sc} = 1.10 - 1.42$), eventually forcing collapse by overdensity. The collapse, as seen from both density and radial velocity plots, proceeds quite classically, in an outside-in manner ($t/t_{sc} = 1.65 - 1.83$).

3.3.4. Intermediate Run 1/30

Unlike the compression wave collapse cases, but similar to the 1/10 case (though not evident in that plot), the BE sphere enters a breathing mode over the first crossing time ($\sim 1 t_{sc}$) as evident by the outward motions of the $t/t_{sc} = 0.95$ radial velocity curve in Figure 8. During this oscillation, we see the interior density ($\xi < 4$) decrease without a concomitant decrease in the BE sphere radius (location of the kink in density), indicating the breathing mode initially vacates mass from the inner regions of the BE sphere. This mass is small relative to the mass of the sphere (recall, $M_{BE} \approx 150M_{\odot}$), only about $0.4 M_{\odot}$. Mass from the sphere is redistributed smoothing out local inhomogeneities. The ambient material then re-equilibrates to a rough HSE. The re-equilibration, however, leaves the the BE sphere in the unstable regime with the non-dimensional radius $\xi > \xi_{crit}$ (Fig. 9). Thus, even numerical noise will be enough to trigger the collapse of the re-configured sphere. For $t > 2.46$, we see the sphere experience the Classic outside-in collapse with supersonic inflows initiated by $t = 2.85$.

4. Discussion

We have found that the collapse of the Bonnor-Ebert sphere strongly depends on the nature of its encompassing medium. For those media with masses and densities (maybe we should be talking about both of these things, in terms of a) jeans unstable environments, and b) timescales for freefall) large enough to collapse on timescales comparable to the BE sphere, strong compression waves can be induced on the surface

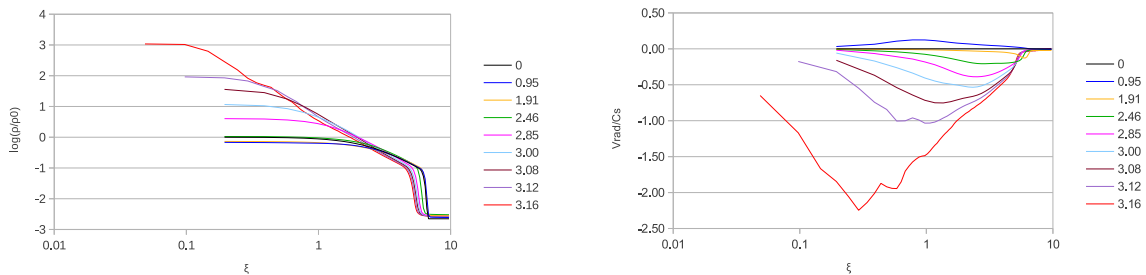


Fig. 8.— Density and radial velocity profiles for Run 1/30, $\rho_{amb} = \rho(R_{BE})/30$. As can be seen in the left density plot and right velocity plot, the BE sphere enters a breathing mode for time states $t/t_{sc} = 0 - 2.46$, where the interior density rises and falls and the radial velocity exhibits small subsonic oscillations. By the next time curve, $t/t_{sc} = 2.86$, gravitational instability has set in and Classic outside-in collapse is underway. Collapse concludes with sink particle formation at $t_{sink}/t_{sc} = 3.16$.

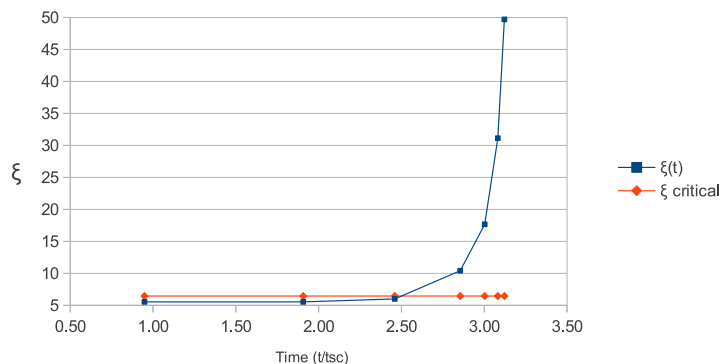


Fig. 9.— Variation of non-dimensional radius with time. Non-dimensional radius (ξ) is calculated for each time state corresponding to Figure 8 according to $\xi = (4\pi G\rho_0/C_s^2)^{1/2}r$ (Eqn. 1), with ρ_0 and r being those instantaneous values of the BE sphere for that time state. Since ρ_0 and r change over the course of the simulation (refer Fig. 8), we see a change in ξ that takes the BE sphere from the sub-critical to super-critical regime by $t/t_{sc} = 2.85$.

of the sphere, mediating its own collapse. For densities low enough, the direct role of the ambient medium is diminished and instead a meager accumulation of ambient mass can be the trigger of collapse. Depending on the mass (density?) of the ambient, early periods of the collapse follow one of two discrete modes. By late times, however, the collapse begins to mimic the classic outside-in profile in all cases. (Why?)

One possible early mode of collapse was a compression wave phase, which was most strongly present in the Matched case. For a sufficiently large ambient medium, the collapse time of the ambient can be approximated by the free-fall time (t_{ff}) of a uniform sphere (Eqn. 6). This time scale for the Matched ambient medium, is calculated to be on the order of the BE sphere’s sound crossing time, t_{sc} ($t_{ff}/t_{sc} \sim 4.3 \text{ Myr}/3.5 \text{ Myr} \sim 1$), indicating that the time needed for the sphere to adjust thermally via sound waves to any gravitational instability induced at its boundary is comparable to the collapse time of the ambient gas. Thus, as the ambient gas collapses, the sphere does not have time enough to equilibrate, indicating that the BE sphere’s own evolution is strongly effected by the evolution of the surrounding ambient medium. Further, a sufficiently large ambient medium that is matched in density with the BE sphere is highly Jeans unstable. That is, the sound crossing time of *the ambient* is much greater than t_{ff} ($t_{sc,amb}/t_{ff} \sim 130$, in our Matched case). Thus, the ambient medium is gravitationally unstable on timescales comparable to the evolution of the BE sphere (don’t know if we want to add this or not). Strongly driven inward motions onto the BE sphere are to be expected, resulting in the complete compression and destruction of the sphere.

In contrast, when the BE sphere was not crushed under compression waves, we found collapse was triggered by the accumulation of in-falling ambient mass. This squeezed the sphere into smaller radii (not sure if this is the right way to put it... sounds like a ram pressure almost), ultimately switching the sphere from being marginally stable to unstable. As an approximation, we measured the effect of a decreasing radius and concomitant increasing central density on the nondimensional radius ξ . We found this was to move ξ to larger and larger values (Fig. 9). Recall that for values of $\xi > 14.1$, BE spheres are unstable to collapse. Thus, as the BE sphere evolved dynamically in response to the mild infall of ambient material, it became more and more susceptible to collapse. So long as the ambient gas’s density was high enough, the sphere eventually collapsed. The case where this was the dominant mode of collapse was for a density ratio of 30, where the relevant time scales were $t_{ff}/t_{sc} \sim 7$ (again, the freefall time is calculated for the ambient medium).

If the density contrast was made high enough, however, we found collapse was not triggered. Instead, under these circumstances the BE spheres remained dynamically stable (as in the Sparse case, $\eta = \rho_{BE}/\rho_{amb} \sim 100$) over many BE sphere crossing times. This indicates a critical value of the ambient density, defining a turnover between too heavy to sustain the the BE sphere, and too light to induce collapse. We ran additional simulations between $\eta = 30$ and $\eta = 100$ to find an η for which collapse was triggered. Within the simulation time t_{sim} (taken to be the t_{sim} used in the $\eta = 100$ stability case), we found that $\eta = 45$ did collapse, but $\eta = 50$ did not. Running the $\eta = 50$ case out a little longer, showed it did eventually collapse. This indicates that the turn-over occurs due to gravitational settling of the ambient material onto the BE sphere. Within some time range, the amount of material that has fallen onto the sphere may or may not be sufficient to induce collapse. Therefore, we can model this system as a settling atmosphere, in order to get an estimate for where the turn-over occurs between stable and unstable configurations. For an isothermal, plane parallel atmosphere, the scale height is given by,

$$h = \frac{K_B T}{m_H g} \tag{7}$$

Assuming g is constant, we can approximate it as,

$$g = \frac{GM_{BE}}{R_{BE}^2} \quad (8)$$

Next we imagine the ambient medium, initially out of hydrostatic equilibrium given its uniform density, begins to fall in toward the surface of the BE sphere. The material which falls down to the surface is shocked, puffs up, and creates an atmosphere in hydrostatic equilibrium of scale height h . This atmosphere induces some pressure on the surface of the BE sphere, which grows with time as the amount of mass that has fallen into the atmosphere increases. The pressure at the surface can then be approximated as,

$$P = F/A = \frac{GM_{BE}M_{atm}(t)}{4\pi R_{BE}^2(R_{BE} + h)^2} \quad (9)$$

To get an approximation for the mass of the atmosphere, $M_{atm}(t)$, we consider the collection of mass parcels that have had time enough to fall down onto the BE sphere from freefall. Considering each parcel of gas in the ambient to only be gravitationally attracted by the BE sphere, the freefall time for each parcel is approximately,

$$t_{ff} = \frac{\pi}{2} \frac{(r)^{3/2}}{\sqrt{2GM_{BE}}} \quad (10)$$

Inverting this equation for the freefall radius gives,

$$r_{ff} = \left(\frac{2\sqrt{2GM_{BE}}}{\pi} t \right)^{2/3} \quad (11)$$

The mass within this freefall radius is then given by,

$$M_{atm}(t) = \frac{4}{3} \pi r_{ff}^3 \rho_{amb} \quad (12)$$

where we take the ambient density ρ_{amb} to be its initial value. Combining this with the pressure expression above yields,

$$P(R_{BE}, t) = \frac{8}{3\pi^2} \left(\frac{GM_{BE}}{R_{BE}} \right)^2 \frac{\rho_{amb}}{(R_{BE} + h)^2} t^2 \quad (13)$$

We used this expression to calculate the pressure perturbation (induced by atmospheric settling) at the BE sphere surface over time. We were only concerned with those ambient media that were Jeans stable, as determined by comparing the Jeans length of the ambient environments to the box size. The reasoning for this was that as the ambient becomes more Jeans unstable, there must be a shift in the dynamics from a gravitational settling to a uniform collapse of the ambient for $r_{box} \gg R_{BE}$. Figure 10 shows that this atmospheric settling model predicts a threshold value at which a sink particle is formed. As the ambient density is decreased ($\eta = \rho(R_{BE})/\rho_{amb}$ increased), the time it takes to reach this threshold grows. Thus, one can predict if/when collapse would be triggered by calculating when the external pressure meets this critical value. The $\eta = 100$ remained dynamically stable over much longer time scales than predicted, as is shown in the figure. This is as expected, however, given the approximation must break down for sparse/hot

enough environments where the scale height becomes much greater than the box, as for the $\eta = 100$ case. Additionally, we found the $\eta = 10$ case does not group with the other cases listed in this figure. The ambient medium in the $\eta = 10$ is only marginally Jeans stable, suggesting this may no longer be in the regime for which this approximation holds. Rather, the dynamics for this, as well as denser ambient cases, are likely more accurately given by a uniform spherical collapse model for the ambient.

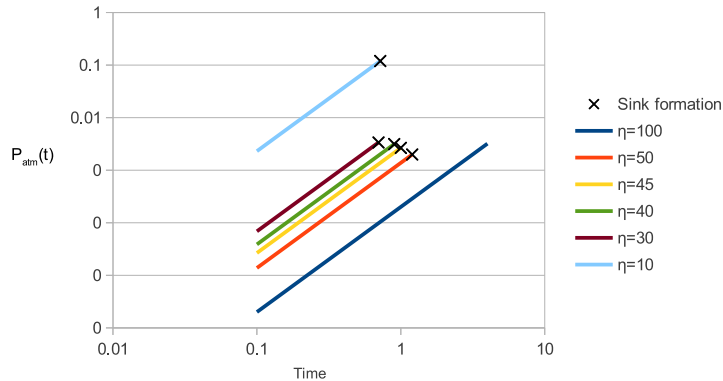


Fig. 10.— Approximating the growth in pressure at the BE sphere surface over time using an atmospheric settling model. The x-axis is time in computational units ($t(\text{sec}) = t \cdot t_{\text{scale}}$, where $t_{\text{scale}} = 5.5e14$), and the y-axis is the pressure induced at R_{BE} from atmospheric settling, $P_{\text{atm}}(t)$, also in computational units ($P(\text{ba}) = P \cdot P_{\text{scale}}$, where $P_{\text{scale}} = 2.77e-13$). Small x’s on the curves indicate if and when a sink particle formed. There is a threshold pressure that is reached by the time a sink particle is formed for sparse cases $\eta_{30} - \eta_{50}$, indicating the approximation is valid when the ambient is not gravitationally dominated ($\eta \leq 10$) and the scale height is within the box limits (see text).

Given there is a cut-off to the induced dynamical instability when the ambient density becomes low enough, we conclude that BE sphere type solutions for isolated starless cores/clumps require high values of the density contrast for them to be long lived. Lower density contrasts imply the clouds are short-lived structures, most likely being part of a region in which collapse is ongoing both locally and globally. Given the rapid crushing of the BE spheres by the infall of highly Jeans unstable environments (I am not sure if this is something we directly tested or emphasized above in results section...), such unmatched density solutions may be the only means for establishing a long-lived core with properties like a BE sphere.

While we found a distinction between the different triggers of collapse (compression waves or matter redistribution) and their time scales, we found little difference in the late phase of evolution (i.e. after collapse has been initiated); the systems that went unstable always resumed classical collapse by sink particle formation. That is, profiles assumed familiar features such as the development of a collapsing core trailed by a r^{-2} envelope, and radial inflow that tracks the core-envelope boundary. Thus, we conclude that the well known features of BE sphere collapse are robust after collapse is sufficiently underway and under the spherically symmetric conditions we and those previous studies have tested. Further, these results provide support for the WS framework in matching the predicted roles of compression waves with the collapse of embedded BE spheres.

Do we want to add anything more? Such as - how these cases match physical reality? Which is more physically realistic? How the Matched case is highly artificial?

5. Conclusions

- Gravitational dynamics (infall or "settling") of the ambient medium can drive BE sphere collapse.
- For those scenarios where collapse is triggered, the time it takes for the sphere to go unstable is inversely proportional to the ambient density.
- BE Spheres driven to collapse by strong compression waves induced by ambient infall eventually progress through the "Classic" outside-in pathway.

6. Future Directions

As a next step for these simulations, it would be interesting to test a more general scenario of embedded BE spheres. For instance, one could place the BE sphere at a region away from the center of mass position of the parent cloud, and with ambient density that varied as a function of angle around the BE sphere. This would be a more accurate model for an isolated core, given they seem to be associated with regions where ambient gas has been dispersed and heated by nearby, heterogeneously positioned H₂ regions (need citation?). It might also be of interest to quantitatively test the link between a set of simulations such as these, and the analytical solutions given by Whitworth & Summers (1985).

7. Appendix

7.1. Self-gravity in AstroBEAR2.0

The Euler equations with self-gravity are given by,

$$\frac{\partial \rho}{\partial t} + \nabla \cdot (\rho \vec{v}) = 0 \quad (14)$$

$$\frac{\partial \rho \vec{v}}{\partial t} + \nabla \cdot (\rho \vec{v} \vec{v} + P) = \rho \nabla \phi_g \quad (15)$$

$$\frac{\partial E}{\partial t} + \nabla \cdot [\vec{v}(E + P)] = -\rho \vec{v} \cdot \nabla \phi_g \quad (16)$$

where ϕ_g is the gravitational potential given by the Poisson's equation,

$$\nabla^2 \phi_g = 4\pi G \rho \quad (17)$$

Written in this form, the equations are conservative with an additional source term vector, \vec{S} , given by the components on the right hand side of equations (14-16). AstroBEAR2.0 solves the system of equations using a Strang split method, solving separately the homogenous versions of the Euler equations (14-16) during hydro steps and the source term equations, $d\vec{u}/dt = s(\vec{u})$ where \vec{u} is the vector of fluid variables, during the source steps. For this method, a source step of half a time step is taken on both sides of the hydro advance

step. The hydro advance steps use one of many available hyperbolic solvers. To specify $\vec{S}(\vec{u})$, Equation 17 is solved using HYPRE (cite), a generalized software package that solves linear systems on massively parallelized computing systems.

- momentum vs energy conserving schemes?

-CTU scheme?

-boundary conditions?

7.2. Testing self-gravity in AstroBEAR2.0

As a test for our self-gravity implementation, we checked whether the code could reproduce the correct growth rate for the Jeans instability. We briefly review the derivation for the growth rate here. The linearized, self-gravitating (1D) fluid equations are given by

$$\frac{\partial \rho'}{\partial t} + \rho_0 \nabla \cdot v' = 0 \quad (18)$$

$$\rho_0 \frac{\partial v'}{\partial t} = -C_s^2 \nabla \rho' - \nabla \phi' \quad (19)$$

$$\nabla^2 \phi' = 4\pi G \rho' \quad (20)$$

where the background density (ρ_0) and gravitational potential (ϕ) is assumed constant, and the velocity is initially zero ($v_0 = 0$) (note this reproduces the classic Jeans swindle, but for our purposes it is safe to ignore this effect). The primed terms in the equations indicate the perturbation in the corresponding variable. By combining these equations, one arrives at the following wave equation in the density perturbation,

$$\frac{\partial^2 \rho'}{\partial t^2} - C_s^2 \nabla^2 \rho' = -4\pi G \rho_0 \rho' \quad (21)$$

Looking for plane-wave solutions to this equation,

$$\rho' \propto e^{ikx - \omega t} \quad (22)$$

gives the dispersion relation,

$$\omega^2 = C_s^2 k^2 - 4\pi G \rho_0 \quad (23)$$

and hence the growth rate of the density perturbation (ω^{-1}). Note that only for, $C_s^2 k^2 - 4\pi G \rho_0 < 0$, are the waves exponentially growing. This length scale defines the Jeans length, and underlines the classical Jeans instability.

To find the corresponding velocity perturbation, we insert the determined density function into the continuity equation. This gives,

$$v' \propto -\frac{\omega}{\rho_0 k} \text{Sin}(kx) \quad (24)$$

The pressure perturbation is then specified using the ideal gas equation,

$$P \propto \frac{K_B T}{m_H} (\rho_0 + \rho') \quad (25)$$

We seeded a 1D grid with these perturbations, of amplitude $\delta = 0.001$, and evolved the domain over 5 e-folding times (the time it takes the perturbation to increase by a factor of 'e') using periodic boundary conditions for both the box and the elliptic solver. The code was able to match the growth rate of the perturbation over the first couple of e-folding times (τ_e), to good accuracy (Fig. Density Perturbation vs. time). By about $t=3 \tau_e$, the rate of growth began to increase beyond the analytical curve (Fig. Slope), remaining within 10%, however, by the end of the simulation. These results confirm AstroBEAR2.0's ability to model self-gravity in astrophysical flows.

7.3. Bonnor-Ebert Sphere Solutions

The equations that specify the parameters of the BE sphere are derived from the equations of self-gravitating hydrodynamics. Combining the condition for hydrostatic equilibrium in spherical coordinates, Poisson's equation for gravity, and the isothermal equation of state,

$$-\frac{\nabla P}{\rho} - \nabla \phi_g = 0 \quad (26)$$

$$-\nabla^2 \phi_g = 4\pi G \rho \quad (27)$$

$$P = \rho C_s^2 \quad (28)$$

where ϕ_g is the gravitational potential, P is the thermal pressure, ρ is the density, and C_s is the isothermal sound speed, yields (cf. Stahler & Palla 2005),

$$\rho(r) = \rho_0 e^{(-\phi_g/C_s^2)} \quad (29)$$

Thus, determination of ϕ_g yields $\rho(r)$ given the central density ρ_0 , where ϕ_g is determined via,

$$\frac{1}{r^2} \frac{d}{dr} \left(r^2 \frac{d\phi_g}{dr} \right) = 4\pi G \rho_0 e^{(-\phi_g/C_s^2)} \quad (30)$$

When equation 30 is made scale-free,

$$\psi = \frac{\phi_g}{C_s^2} \quad (31)$$

one gets the *Lane-Emden* equation for an isothermal sphere,

$$\frac{1}{\xi^2} \frac{d}{d\xi} \left(\xi^2 \frac{d\psi}{d\xi} \right) = e^{(-\psi)} \quad (32)$$

There are two classes of solution to this equation when one assumes an isothermal equation of state. The first is the asymptotic solution, known as the *singular isothermal sphere* (SIS). It represents a sphere of infinite central density and radius given by,

$$\rho = \frac{C_s^2}{2\pi G} r^{-2} \quad (33)$$

This class of solution was used by Shu to study inside-out collapse (Shu 1977). The second class of solutions are the Bonnor-Ebert spheres. These are the regular solutions of the isothermal Lane-Emden equation that are found by numerical integration with the boundary conditions $\psi(0) = 0$ and $\psi'(0) = 0$. Each BE sphere is specified by a different truncation radius R_{BE} and central density ρ_0 , and each is characterized by a different bounding external pressure P_{ext} .

REFERENCES

- Alves, J. F., Lada, C. J., & Lada, E. A. 2001, , 409, 159
- Anathpindika, S., & Di Francesco, J. 2013, MNRAS, 430, 154
- Banerjee, R., Pudritz, R. E., & Holmes, L. 2004, MNRAS, 355, 248
- Bonnor, W. 1956, MNRAS, 116, 351
- Carroll-Nellenback, J., Shroyer, B., Frank, A., & Ding, C. 2011, ASP Conference Series
- Cunningham, A. J., Frank, A., Varnière, P., Mitran, S., & Jones, T. W. 2009, ApJS, 182, 519
- Ebert, R. 1955, Z. Astrophys, 37, 217
- Federrath, C., Banerjee, R., Clark, P. C., & Klessen, R. S. 2010, ApJ, 713, 269
- Foster, P. 1994, , 65, 105
- Foster, P. N., & Chevalier, R. A. 1993, ApJ, 416, 303
- Hennebelle, A. P., Whitworth, A. P., Gladwin, P. P., & Andre, P. 2003, MNRAS, 340, 870
- Hunter, C. 1977, ApJ, 218, 834
- Larson, R. 1969, MNRAS, 145, 271
- Liu, F. K. 1996, MNRAS, 281, 1197
- Myers, P. C. 2008, ApJ, 687, 340
- Penston, M. 1969, MNRAS, 144, 425
- Shu, F. H. 1977, ApJ, 214, 488

Shu, F. H., & Adams, F. 1987, , 122, 7

Shu, F. H., Lizano, S., & Adams, F. 1987, , 115, 417

Spitzer, L. 1968, *Nebulae and Interstellar Matter* (The University of Chicago Press), 44

Stahler, S., & Palla, F. 2005, *The Formation of Stars* (Wiley-VCH), 242–245

Truelove, J., Klein, R. L., McKee, C. F., Holliman, J. H., Howell, L. H., & Greenough, J. A. 1997, *ApJ*, 489

Ward-Thompson, D., Andre, D., Crutcher, P., Johnstone, D., Onishi, T., & Wilson, C. 2007, *Protostars and Planets V* (Tucson: Univ Arizona Press), 33

Whitworth, A., & Summers, D. 1985, *MNRAS*, 214, 1